Chapter-V

$BaZr_{0.4}Ti_{0.6}O_3$/Poly(Vinylidene fluoride) Composite Films with Improved Dielectric and Energy Storage Properties

5.1 Introduction

With the development of Science and technology, the life style of human beings has been improved and the overpopulation on the earth has caused energy depletion. In near future, fossil fuel is going to exhaust and continuously increasing energy demand can cause energy crisis across the world. Although, many energy saving devices are being already used, most of them are made up of lead based materials which is very dangerous for human being and environment. To overcome the global problems from energy depletion without lead pollution, lead free materials for energy storage have been most important options [206–209] . There are several types of energy storage devices like fuel cells, batteries, super capacitors and dielectric capacitors. Fuel cell contain high energy density and low power density which is not much suitable for hybrid electric vehicles or pulsed power applications. Dielectric capacitors have been used in power systems of hybrid electric vehicles and many other fields depending upon the material state and operating range of temperature [210]. Thus, if the energy storage capacity of the dielectric capacitors can be improved in comparison to fuel cells or even batteries, their application area can be greatly expanded. Ceramic materials in thick film form represents better electrical breakdown strength and reliability in comparison to bulk ceramics due to its low defects which is essential criteria for a material to be used for energy storage applications [211]. With the development and continuously increasing demand of portable devices, researchers have focused their attention on flexible materials that promotes polymer dielectric materials in last few decades[212]. Polymers have many applications in energy harvesting, energy conversion, energy storage and dielectric capacitors [2,39] . In general, polymers posses high dielectric breakdown strength, low dielectric constant and low polarization value which limits their application in high energy storage application. Among the various known polymers like polypropylene, polyamide, polyester, epoxy resin, poly(methyl methacrylate),

Polyvinylidene difluoride (PVDF), aromatic polyurea etc. researchers have focused their attention on PVDF polymer due to its ferroelectric nature and high dielectric constant value among all the polymers [39,213]. Various researchers have explored polymer nanocomposites to overcome the problem of low polarization, thermal stability and dielectric permittivity value of polymers [214] . In general, ceramics have high dielectric constant but have inflexible and possess low electrical breakdown strength while polymers can be easily processed in different shapes. In this regard, Polymer ceramic nanocomposites have been developed as next stage energy storage materials by reinforcement of ceramic nanoparticle filler in the polymer matrix with the advantage of high value of dielectric constant and good thermal stability of ceramics. These nanocomposites have been synthesized by choosing ceramic nanoparticles of high dielectric constant and polymers of high electrical breakdown strength and flexible nature with improved energy storage properties and reduced weight of electric and electronic devices [17,215–217]. Theoretically, It has been proved that the properties of interface between polymer matrix and filler in the composites is dominant at nanometer scale [68]. Still, these composites have some limitations to overcome such as particle agglomeration, leakage current, high local fields, nonuniform particle dispersion and dielectric loss. In this regard, surface modification of fillers with various coupling agents have been performed to decrease agglomeration and improve particle dispersion. Increasing dielectric constant and dielectric breakdown strength of dielectric material simultaneously is the main path to achieve high energy density which is generally contradictory.

In the present research work, we have used PVDF polymer and $BaZr_{0.4}Ti_{0.6}O_3$ ceramic for synthesizing Polymer ceramic nanocomposite. PVDF polymer is ferroelectric in nature and have highest dielectric constant among all known ferroelectric polymers [2]. PVDF is semicrystalline in nature having four crystalline phases namely α (nonpolar) β (polar form

of α phase), γ(polar) and δ(Polar) [218]. Dielectric ceramics used in present composite is $BaZr_{0.4}Ti_{0.6}O_3$ (BZT) which is nonlinear and relaxor ferroelectrics in nature [219]. Energy storage behaviour in relaxors has received much attention due to its large saturation polarization, rapid discharge rate and small remnant polarization. The nonlinear behavior of dielectric materials is due to the switching of ferroelectric domains. Relaxor ferroelectrics have improved thermal stability in comparison to normal ferroelectrics due to the diffuse phase transition. BZT relaxor ferroelectrics have attracted much attention due to their moderate permittivity, low dielectric loss, high tunability and chemical stability. Researchers have shown improved dielectric constant and energy storage property in Polyvinylpyrrolidone (PVP) functionalized $BaZr_{0.3}Ti_{0.7}O_3$ (BZT3) nanofibers based PVDF composites[9]. Reported BZT3 nanofibers has been synthesized by electrospinning technique that cannot produce nanofibers in larger quantities, hence commercially not suitable. Here, we have developed as synthesized BZT based PVDF composites and H_2O_2 modified BZT based PVDF composites in film form by taking 10 wt. % of BZT4 ceramic as filler and 90 wt. % of PVDF polymer as matrix via solution casting method. We have synthesized pure PVDF film also with same method to compare the properties. Here we have chosen BZT ceramics for composites because of its higher dielectric constant. The particle size of fillers in polymer composites plays very important role during charge transport phenomena at the interfaces of filler and polymer matrix. Here, efforts have been made to synthesize BZT with reduced particle size using high energy nano milling synthesis process and this BZT ceramic has been used as filler in PVDF polymer matrix to synthesize nanocomposites with improved energy storage properties.

5.2 Synthesis of BZT/PVDF composite film

First BZT ceramic was synthesized using conventional solid state reaction method using high energy ball mill. Raw materials were taken in stochiometric ratio, mixed in acetone

medium and milled in high energy ball mill using zirconia balls at 300 rpm for 12 hr. After milling, the mixture was dried at 80 ^{0}C and calcined at 1200 ^{0}C for 2 hr at 3^0/min to get pure phase of BZT powder. These calcined powders were milled again for 12 hr with 3 mm nanoball in high energy ball mill to get nanocrystalline ceramic powder. Surface modification of BZT powder was performed using 30 vol.% of H_2O_2 solution. For this purpose, grinded BZT powder was refluxed in H_2O_2 solution at 106 ^{0}C for 6 hr and then dried at 120 ^{0}C for 12 hr.

BZT/PVDF and hy-BZT/PVDF nanocomposite films were synthesized using solution casting method with 10 wt. % of ceramic filler and 90 wt. % of polymer matrix. In this method, filler nanoparticles were dispersed in 5 ml DMF solution with the help of ultrasonicator and after that this dispersed nanoparticle in DMF solution was put on magnetic stirrer for 1 hr at 60 ^{0}C. At the same time, PVDF polymer was dissolved in 10 m DMF solution and put on magnetic stirrer for 1 hr at 60 ^{0}C. After that, both solutions were mixed together and put on magnetic stirrer for 8-12 hr at 70 ^{0}C until it converts in thick and homogeneous solution that was further ultrasonicated for 20 minutes. After ultrasonication, above viscous solution was casted on a petri dish and put in a oven at 120 ^{0}C for evaporation of solvent. Thus, we get thick film form of BZT/PVDF composite film. Exactly same process was applied with hydroxylated BZT ceramic and without BZT ceramic for synthesis of hy-BZT/PVDF composite and pure PVDF film respectively. Flowchart for synthesis of BZT powder is shown in Fig. 5.1 and synthesis process of BZT/PVDF composite film is shown in Fig. 5.2.

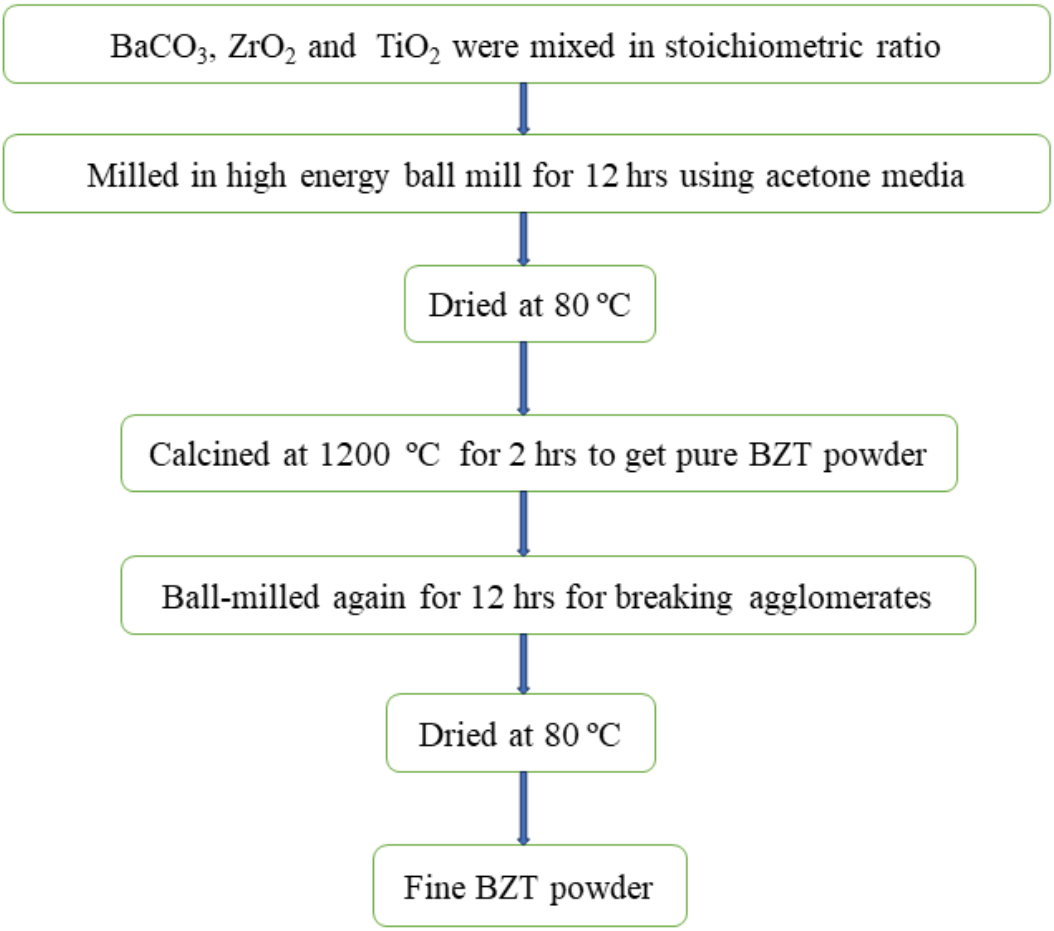

Fig. 5.1 Flow chart for synthesis of BZT powder using high energy ball mill

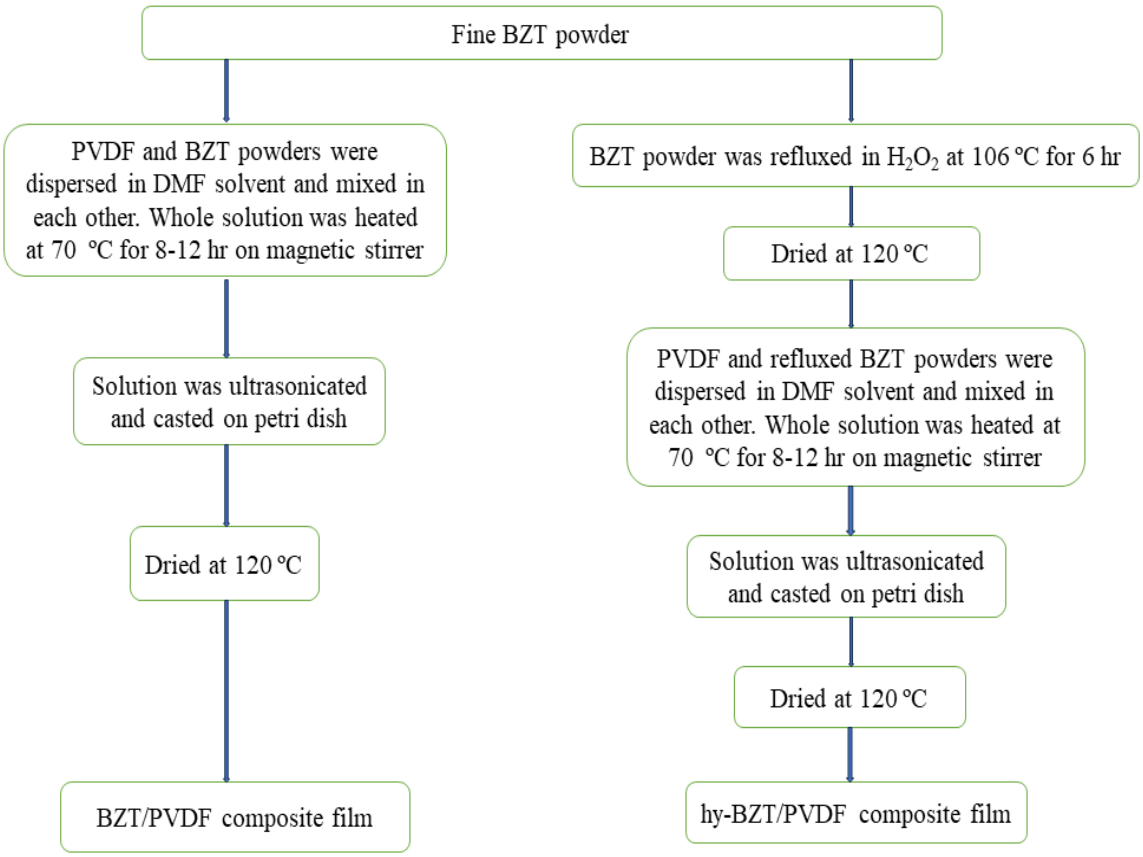

Fig. 5.2 Synthesis process of BZT/PVDF and hy-BZT/PVDF powders using solution casting method

5.3 Results and Discussion

X-ray diffraction analysis was performed using Rigaku Miniflex 600 X-ray diffractometer for structural investigation. Fourier transform infrared (FTIR) spectroscopy was studied to verify the successful hydroxylation of BZT using Thermo Fisher Scientific spectrometer. TGA/DSC analysis was carried out to check the stability and crystallinity of the composites. Dielectric properties were measured with the help of Keysight E4990A, impedance analyzer using air dried silver paste. Polarization Electric field (P-E) hysteresis loop analysis was carried out at room temperature using ferroelectric hysteresis loop tracer with the help of bipolar sine wave Ac-signal. Dielectric breakdown strength measurement was carried out using AC voltage source setup and Weibull analysis was performed.

5.3.1 X-ray Diffraction Analysis

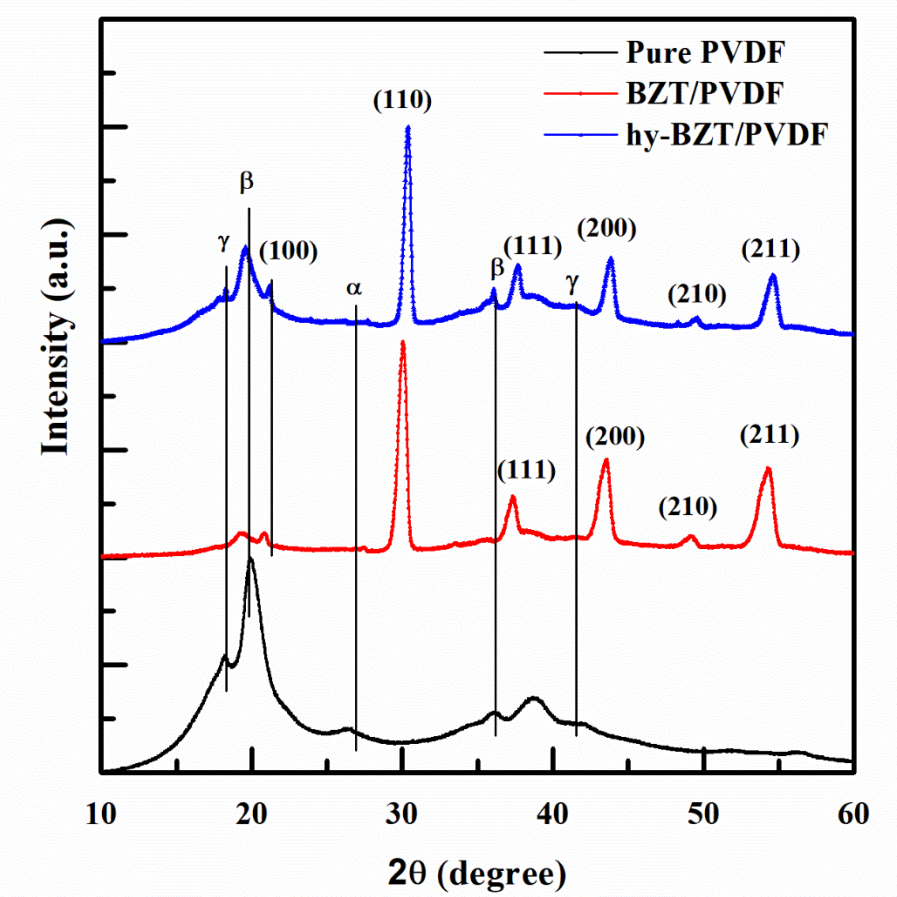

Fig. 5.3 XRD pattern of Pure PVDF film, BZT/PVDF and hy-BZT/PVDF composites

XRD patterns of pure PVDF film, BZT/PVDF composite and hy-BZT/PVDF composite films were recorded to know the crystalline state of composites and are shown in Fig. 5.3. The X-ray diffraction patterns of these films shows that there are different mixed phases namely α, β, γ of PVDF present in the film. The peaks at 2θ in all the films that corresponds to 19.9^0, 26.5^0 are assigned as α phase, 36.2^0 are assigned as β phase and 18.2^0, 38.8^0 are assigned as γ phase of PVDF polymer[107,143,220,221]. The peaks at 2θ in composite films that corresponds to 21^0 (100),30^0 (110), 38^0 (111),44^0 (200), 49^0 (210),54^0 (211) are assigned as BZT with perovskite structure [219,222]. XRD pattern of composite films are associated with the peaks corresponding to PVDF polymer as well as peaks corresponding to BZT ceramic powder that confirms the successful formation of composite films. The peaks

corresponding to PVDF polymer is of relatively low intensity in comparison to BZT ceramics, thus less intense PVDF polymer peaks are observed in composites with highly intense peak corresponding to BZT ceramic.

5.3.2 FTIR Analysis

Fourier transform infrared (FTIR) spectroscopy was performed to determine the functionalization of the BZT ceramic powder. FTIR spectra was recorded for hydroxylated BZT powder, pure PVDF film, BZT/PVDF and hy-BZT/PVDF composite films. The absorbance peaks corresponding to -OH group at 1635 cm^{-1} and 3435 cm^{-1} were found in FTIR spectra of hydroxylated BZT which confirms the successful hydroxylation of BZT ceramic nanoparticles [186,223]. FTIR spectra of hydroxylated BZT powder shows peaks at 578 cm^{-1} which corresponds to vibrations of TiO_6 octahedra[224]. FTIR spectra of pure PVDF, BZT/PVDF and hy-BZT/PVDF consist of α, β and γ phases out of which β and γ phases are dominant that can be clearly seen in Fig. 5.4. Absorption peaks corresponding to wave number 1400 cm^{-1} is recognized as nonpolar α phase while absorption peaks at wave number 1071 cm^{-1}, 1170 cm^{-1} and 836 cm^{-1}, 876 cm^{-1}, 1231 cm^{-1} are assigned as β and γ phases respectively [59,221].These observed data are in consistent with the previously reported data on PVDF film.

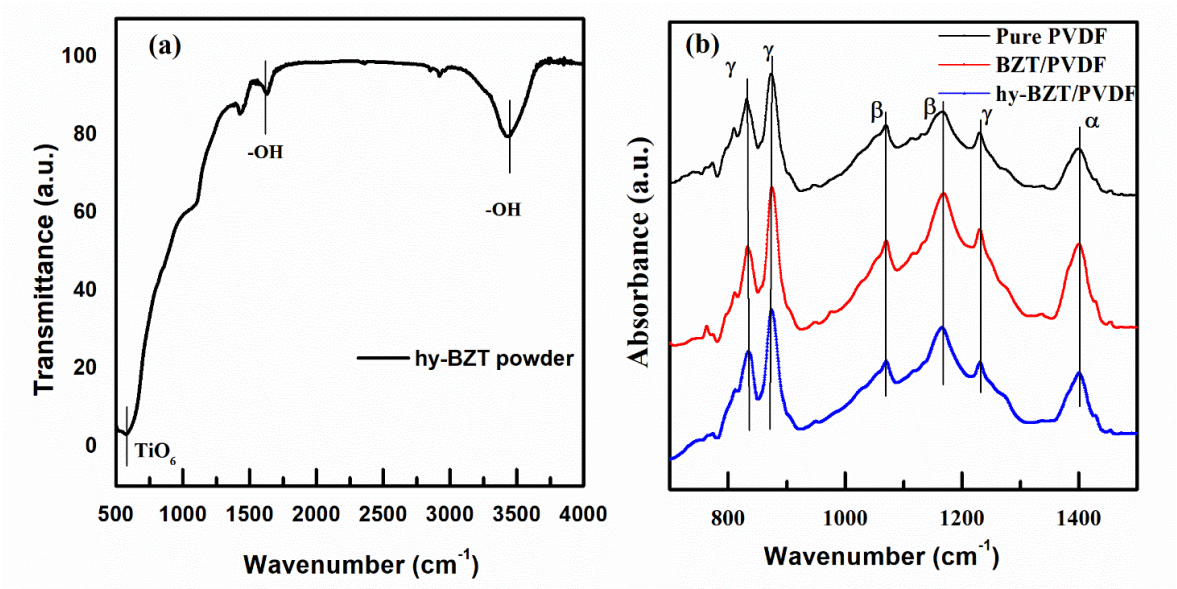

Fig. 5.4 FTIR spectra of (a) hydroxylated BZT powder, (b) pure PVDF, BZT/PVDF and hy-BZT/PVDF composite

5.3.3 Thermal analysis using TGA and DSC

Thermal stability and weight loss of pure PVDF, BZT/PVDF and hy-BZT/PVDF composite films were analyzed using Thermo gravimetric analysis (TGA) curve of respective films which are shown in Fig. 5.5. There was no weight loss observed upto 430^0C, 450^0C and 460^0C in heat treatment process and after that weight loss of 83%, 73% and 69% was observed for pure PVDF, BZT/PVDF and hy-BZT/PVDF composite film respectively. Thus we can predict that composite films are more stable and relatively low weight loss was observed in comparison to pure PVDF film. A steep declination in the weight was observed in the temperature range of 430^0C-500^0C due to pyrolysis of PVDF polymer which results in dissociation of ceramic filler from the polymer matrix. TGA results are in consistent with the previous reported results of PVDF based nanocomposites [107,141].

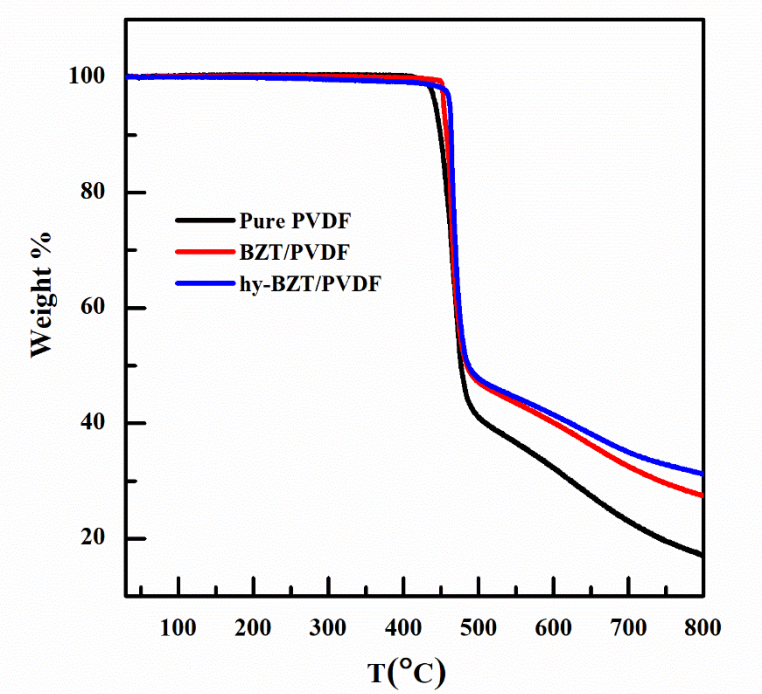

Fig. 5.5 TGA curve of pure PVDF, BZT/PVDF and hy-BZT/PVDF composite

Differential scanning calorimetry (DSC) was carried out to know the idea about crystalline nature and endothermic or exothermic nature of composite film on heat treatment. DSC curve shown in Fig. 5.6 shows the endothermic nature of films and the area under this endothermic peak is directly proportional to degree of crystallinity. In the DSC plot, we see that the area under the curve for composite films is higher than the pure PVDF film thus we can conclude that degree of crystallinity has been increased in case of composite films. An endothermic peak was observed at 167^0C in DSC plot of pure PVDF film and hy-BZT/PVDF composite film which is due to the melting of electroactive β and γ phases of PVDF polymer and also weak endothermic peak was observed at 160 ^{0}C in DSC plot of pure PVDF film which is due to the melting of α phase [188,189]. Thus we can conclude that suppression of α phase happens in case of composite films. In DSC plot of BZT/PVDF composite, an endothermic peak was observed at 169^0C which might be due to the increment in electroactive β, γ phase that results in higher melting temperature.

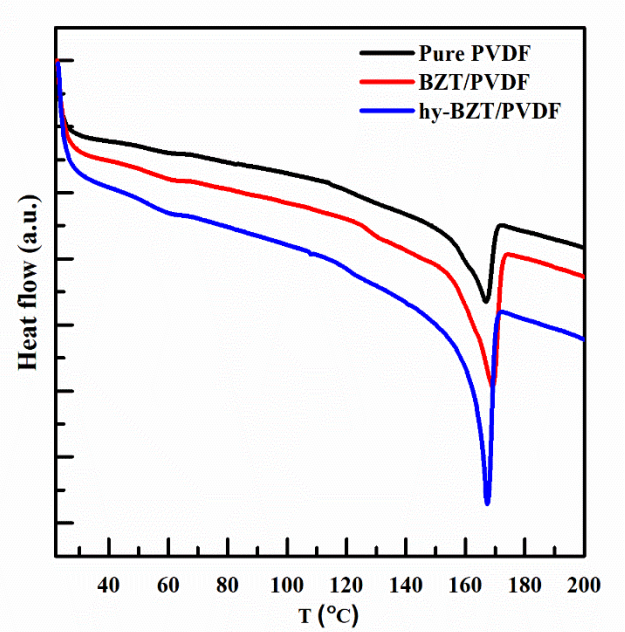

Fig. 5.6 DSC curve of pure PVDF, BZT/PVDF and hy-BZT/PVDF composite

5.3.4 Microstructural Analysis

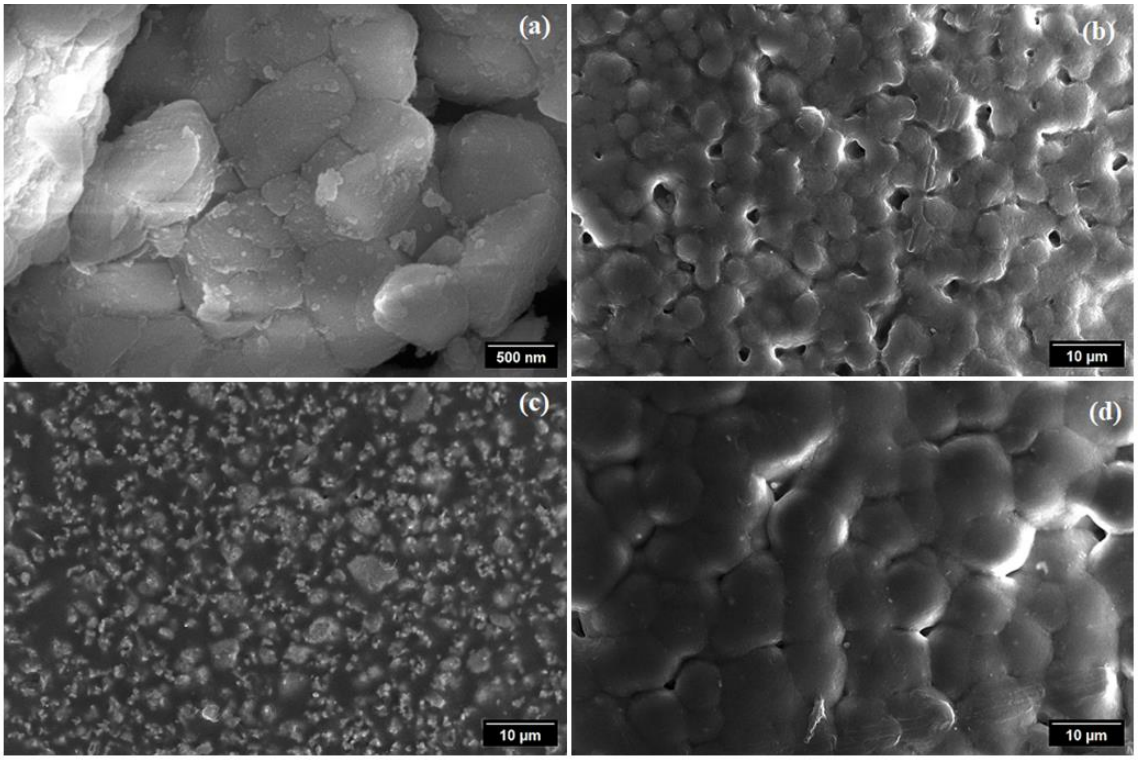

Fig. 5.7 FESEM image of (a) hy-BZT powder, (b) PVDF film, (c) BZT/PVDF film, (d) hy-BZT/PVDF composite film

Surface morphology of pure PVDF film and composite films has been analyzed using FESEM micrograph as shown in Fig. 5.7. Fig. 5.7(a) represents FESEM micrograph of hy-BZT nanopowder and its average particle size is found to be 50 nm using Image J software.

Here, particles seen in the image are in bigger size which is agglomerated form of smaller particles. In Fig. 5.7(b) spherulites are observed in case of pure PVDF film. In Fig. 5.7(c) spherulites are clearly not visible in case of BZT/PVDF nanocomposite film and nonuniform distribution of ceramics in PVDF polymer matrix is observed due to agglomeration of ceramic particles. In Fig. 5.7(d) spherulites are clearly visible in case of hy-BZT/PVDF nanocomposite film, porocity has been minimized and spherulites are in bigger size in comparison to pure PVDF which suggest that nucleation and grain growth process happens at nanofiller site. The FESEM result indicate that there is stronger interaction between PVDF polymer and hy-BZT nanoparticles in comparison to PVDF polymer and BZT nanoparticles. Thus better compatibility between hy-BZT nanoparticles and PVDF polymer is originated due to surface hydroxylation of BZT nanoparticles using H_2O_2. Some potholes are observed in PVDF film and hy-BZT/PVDF nanocomposite films in Fig 5.7 (b,d). It may be due to the bubbles created between the glass and films during synthesis process. The presence of Ba, Zr, Ti and O can be observed in hy-BZT/PVDF nanocomposite film using elemental mapping analysis which is shown in Fig. 5.8.

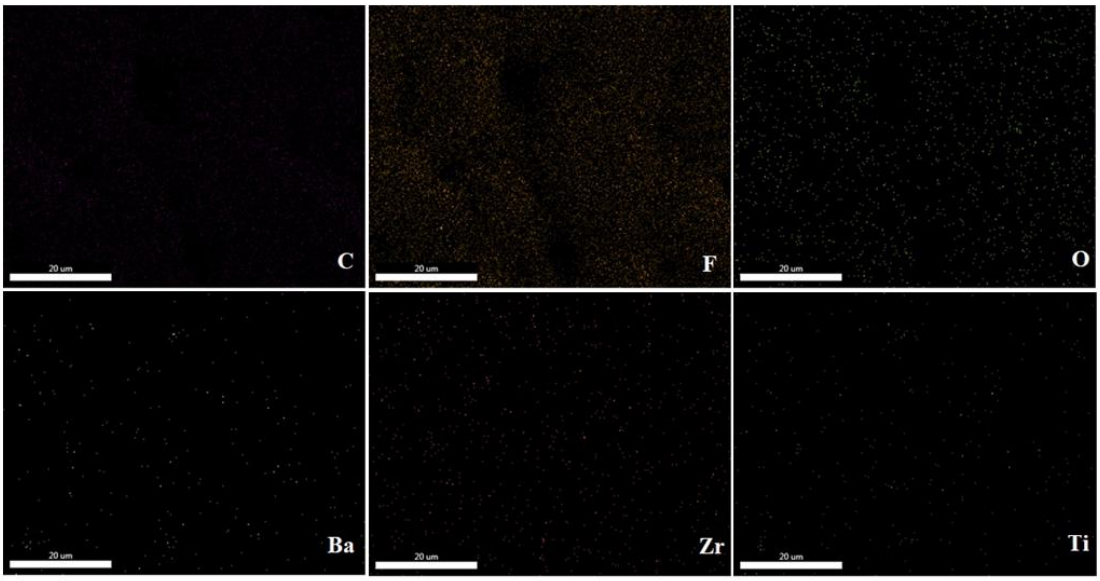

Fig. 5.8 Elemental mapping of hy-BZT/PVDF composite film

5.3.5 Atomic Force Microscopy Analysis

The Fig. 5.9 depicts an Atomic Force Microscopy (AFM) image presenting a 3D plot of PVDF, BZT/PVDF, and hy-BZT/PVDF nanocomposite films. In Fig. 5.9, the film's surface roughness is clearly observable. For in-depth analysis, we employed Nova Px 3.0.4 rev software to illustrate the roughness characteristics, as depicted in Fig. 5.10. Comparatively, pure PVDF exhibits greater roughness than PVDF-based nanocomposites. The roughness of the BZT/PVDF film seems slightly elevated compared to the pure PVDF film and the hy-BZT/PVDF nanocomposite film, possibly due to the nonuniform distribution of BZT nanoparticles in the PVDF matrix. The roughness of the hy-BZ/PVDF nanocomposite film is lower than that of the BZT/PVDF film, attributed to the uniform distribution of BZT particles in the PVDF matrix. However, it is higher than the pure PVDF film due to an increased average grain size, as evident in the FESEM image. Root mean square roughness (Rrms) measurements reveal that PVDF has an Rrms of 6.5 nm, while BZT/PVDF and hy-BZT/PVDF nanocomposite films have Rrms values of 14.5 nm and 9.9 nm, respectively, as indicated by the yellow line in the inset of Fig. 5.10 (a-c).

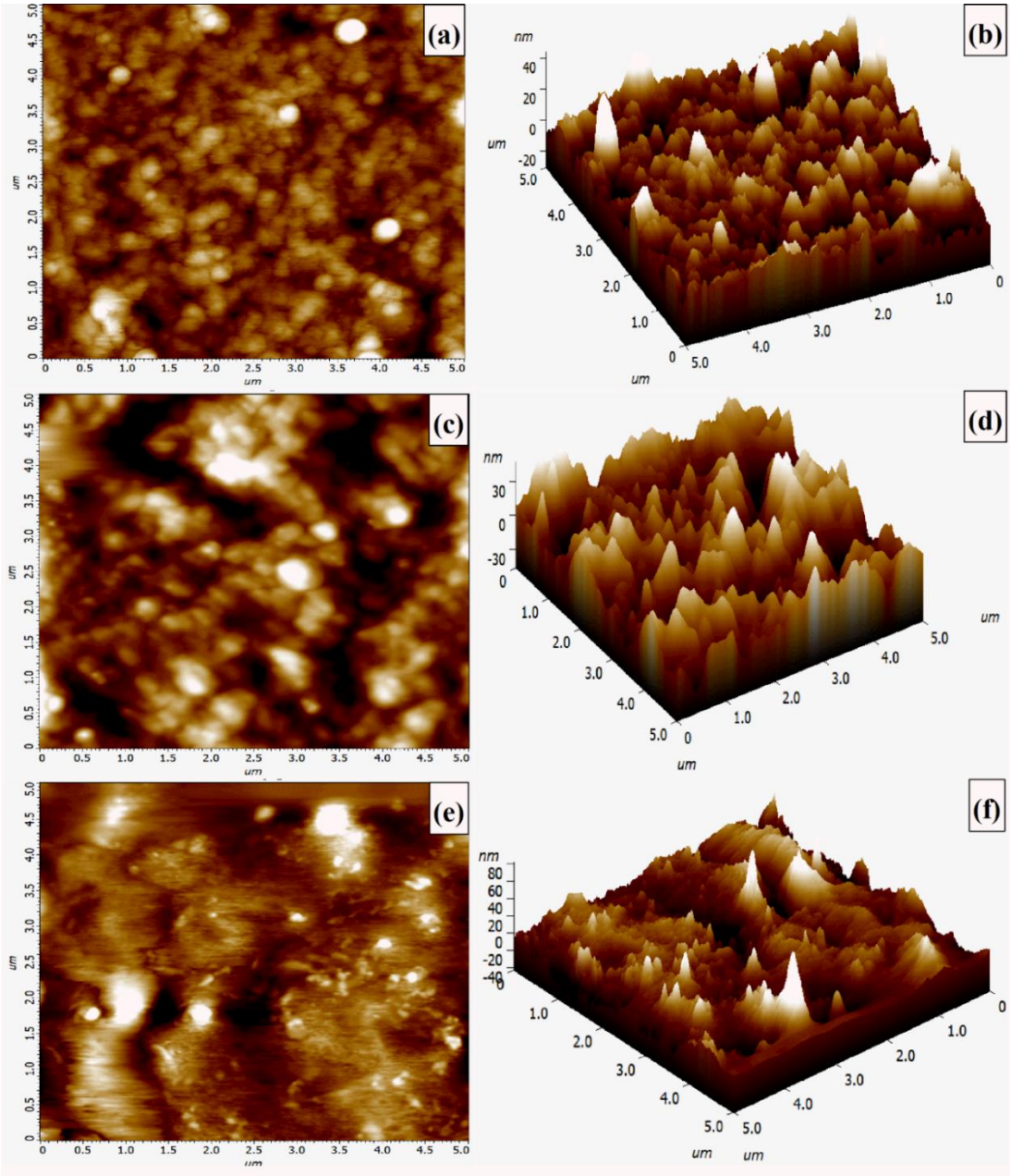

Fig. 5.9 (a) AFM micrograph (5x5 μm) of Pure PVDF film, (b) 3D AFM micrographs (5x5 μm) of Pure PVDF, (c) AFM micrograph (5x5 μm) of BZT/PVDF film, (d) 3D AFM micrographs (5x5 μm) of BZT/PVDF film, (e) AFM micrograph (5x5 μm) of hy-BZT/PVDF film, (f) 3D AFM micrographs (5x5 μm) of hy-BZT/PVDF film

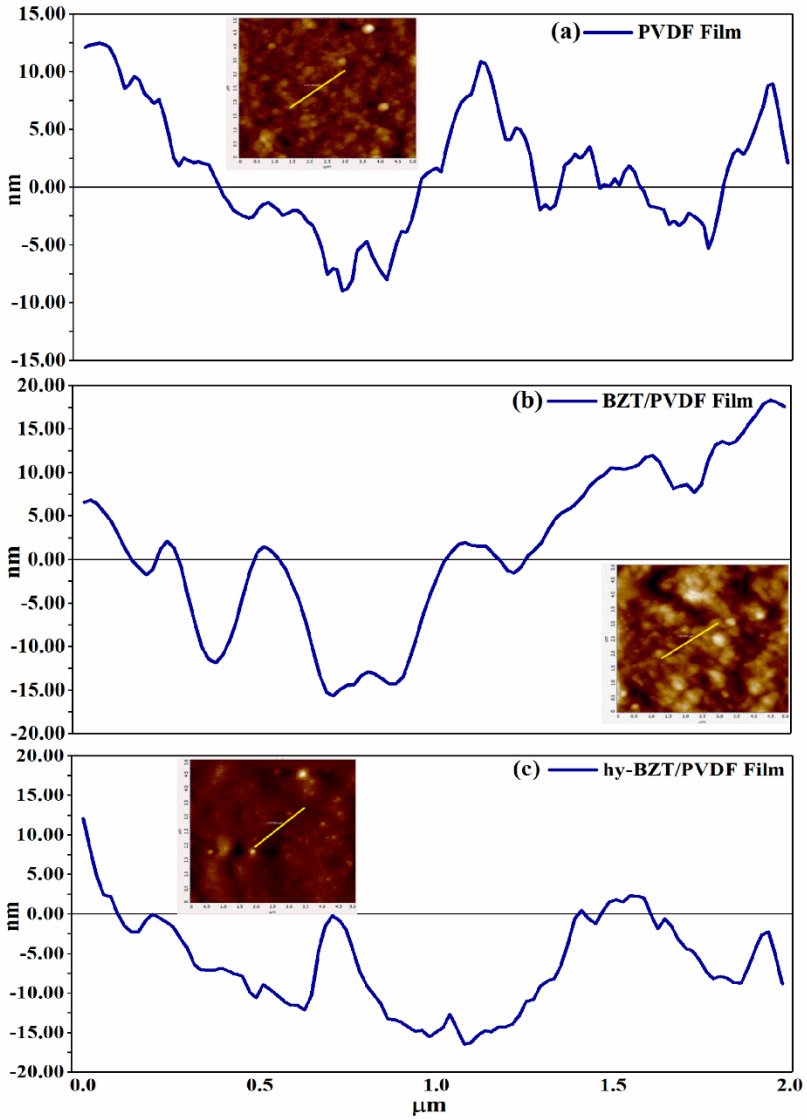

Fig. 5.10 Roughness profile of (a) Pure PVDF film, (b) BZT/PVDF, (c) hy-BZT/PVDF film

5.3.6 Dielectric properties

The dielectric properties have been studied for pure PVDF film, BZT/PVDF and hy-BZT/PVDF composite films. The dielectric constant and dielectric loss value was measured for above mentioned films with the variation of temperature and frequency. The dielectric constant and dielectric loss vs. temperature plot have been shown at 1kHz frequency in Fig. 5.11. It can be seen that the dielectric constant of BZT/PVDF composite films has been increased in comparison to pure PVDF film and further increment in the value of dielectric constant was observed in case of hy-BZT/PVDF composite film in comparison to

BZT/PVDF composite film due to increment in the space charge polarization effect between the ceramic filler and polymer matrix with almost same dielectric loss as in case of pure PVDF film and BZT/PVDF composite film at room temperature. The increment in the value of dielectric constant and dielectric loss was observed with increasing value of temperature for all the films but at the same time, more increment in the value of dielectric loss was also observed in case of hy-BZT/PVDF composite film at higher temperatures. The increment in the value of dielectric constant with temperature is due to the increment in the value of mobility of polar molecules and interfacial interaction between nanofillers at higher temperature [225–228].

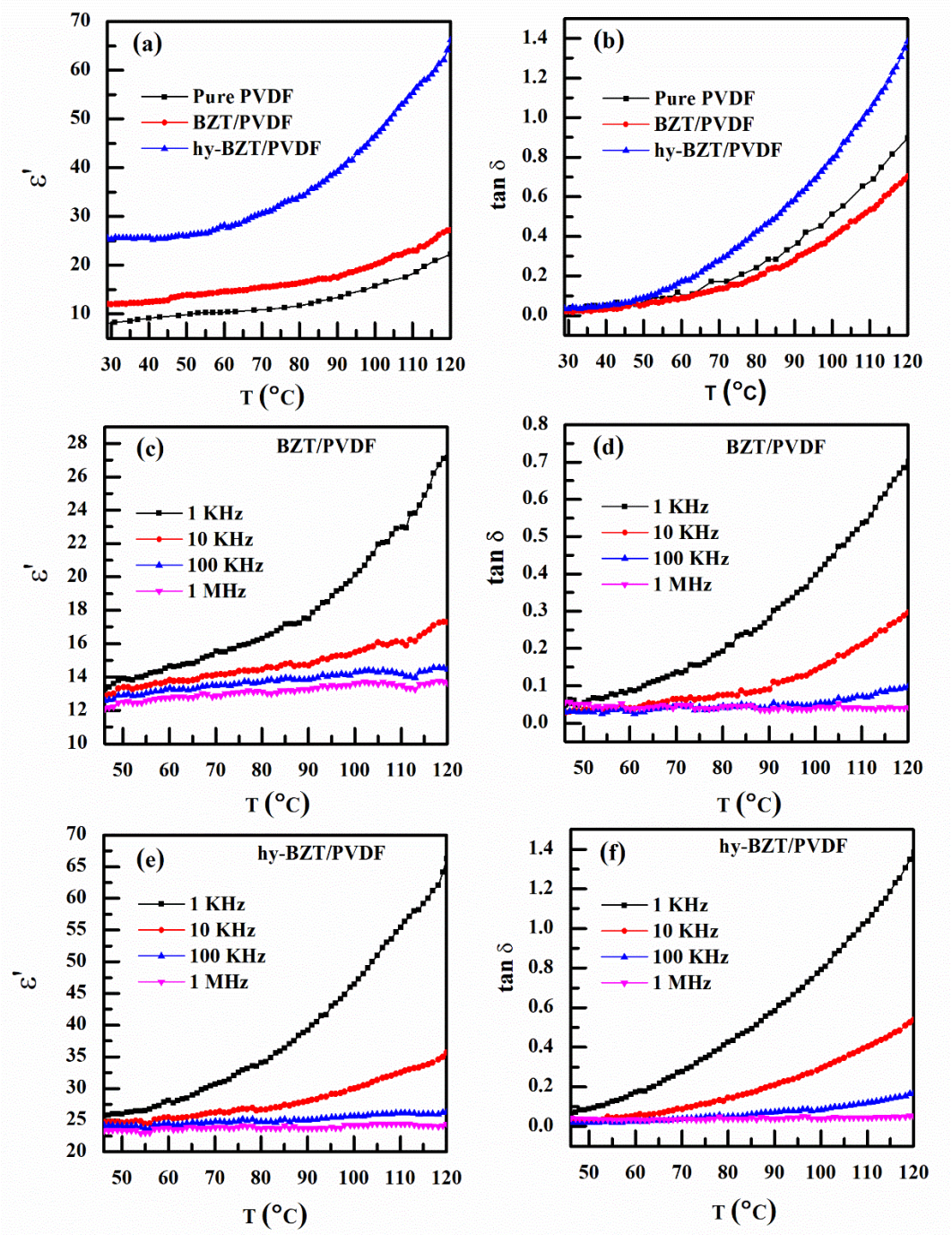

Fig. 5.11 Variation of dielectric constant and dielectric loss with temperature (a),(b) for pure PVDF, BZT/PVDF and hy-BZT/PVDF composites, and at different frequencies for (c),(d) BZT/PVDF composite and (e), (f) hy-BZT/PVDF composite

Fig 5.11 shows variation of dielectric constant and dielectric loss (loss tangent) for BZT/PVDF and hy-BZT/PVDF composite film with temperature at different frequencies respectively. The dielectric constant and loss tangent decreases with increasing frequency due to reduction in interfacial polarization at the interface of heterogeneous system and

decrement in the number of aligned dipoles in electric field direction at higher frequency. The major contribution in dielectric loss is generally due to leakage current in interfacial polarization at lower frequencies and relaxation polarization dielectric loss at higher frequencies [226,227]. Reinforcement of fillers in PVDF polymer matrix having heterogeneous systems with different dielectric materials results in extra polarization due to extra polarization groups under the application of an external electric field [201]. Thus nanocomposite films shows higher dielectric constant due to generation of micro capacitors in composite films during reinforcement of filler in the polymer matrix and reinforcement of fillers also creates large number of free charge carriers [229].

5.3.7 P-E hysteresis loop analysis

The polarization-electric field (P-E) hysteresis curve was analyzed for pure PVDF, BZT/PVDF and hy-BZT/PVDF composite film at 40 Hz frequency to get the idea about energy storage density of above PVDF based composite films and is shown in Fig. 5.12. From the PE hysteresis loop, we can see that the value of maximum polarization has been increased from 0.81 in case of pure PVDF film to 0.98 for hy-BZT/PVDF composite film at applied external electric field of 790 kV/cm because of interfacial interaction of hy-BZT and PVDF polymer and has been listed in table 5.1.

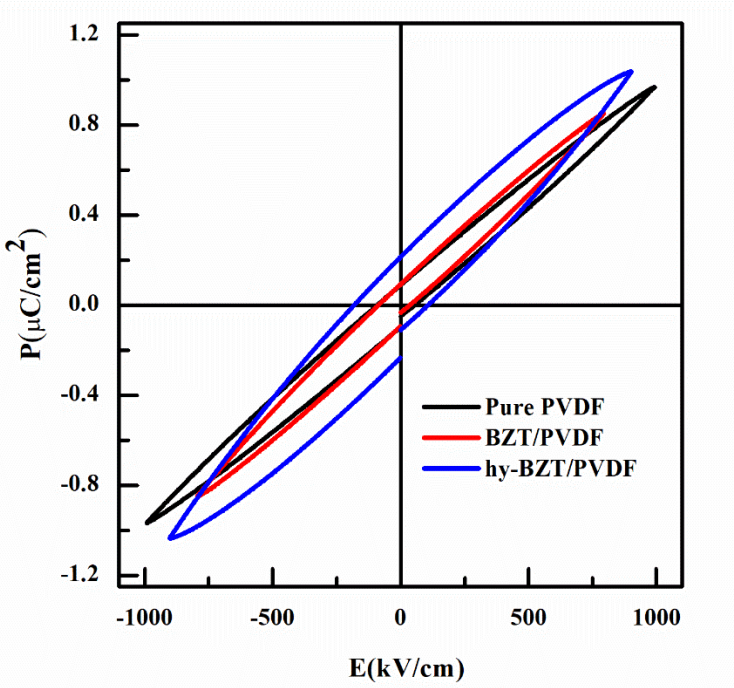

Fig. 5.12 PE hysteresis loop for pure PVDF, BZT/PVDF and hy-BZT/PVDF composite

Table 5.1: Remnant Polarization (P_r) , Maximum Polarization (P_m), Energy storage density (U_e) and discharge efficiency (η) of pure PVDF film, BZT/PVDF and hy-BZT/PVDF composite film

S. No.	Sample Name	Remnant Polarization P_r ($\mu C/cm^2$)	Maximum Polarization P_m ($\mu C/cm^2$)	Energy Storage density U_e (J/cm^3)	Discharge efficiency η (%)
1.	Pure PVDF	0.08	0.81	0.32	86
2.	BZT/PVDF	0.09	0.85	0.37	78
3.	hy-BZT/PVDF	0.20	0.98	0.41	68

5.3.8 Study of breakdown strength using Weibull Analysis

The breakdown strength measurement was performed for pure PVDF film, BZT/PVDF film and hy-BZT/PVDF composite film with the help of ac electric breakdown experimental setup. For this purpose, 8 samples of each film were taken and same ac electric breakdown experiment was performed on it and value of ac breakdown voltage was

measured for each sample. Weibull analysis was performed to calculate the ac breakdown strength of pure PVDF film, BZT/PVDF and hy-BZT/PVDF composite film using Weibull cumulative probability function given by below equation [230,231]

$$P(E) = 1 - \exp[-(\frac{E}{E_b})^{\beta}] \quad (5.1)$$

where P(E) is known as cumulative prospect of electric breakdown strength, E is the actual breakdown strength and E_b is the breakdown strength at 63.2 % of cumulative prospect and β is known as Weibull modulus or shape parameter which can be determined by linear fitting of breakdown field of samples. The plot has been drawn between two parameters which are given by equation (5.2) and (5.3) by assigning the sample number with their breakdown strength in increasing order and is shown in Fig. 5.13.

$$X_i = \ln (E_i) \quad (5.2)$$

$$Y_i = \ln[-\ln(1-\frac{i}{n+1})] \quad (5.3)$$

where Xi and Y_i denote the Weibull distribution function parameters, n is the total number of samples measured and i represent i^{th} number of sample with their increasing order of breakdown strength [232]. Ei is the measured breakdown field of the i^{th} sample. The plot has been drawn between X_i and Y_i with linear fitting of experimental data and value of dielectric breakdown strength and shape parameter has been determined. The dielectric breakdown strength for BZT/PVDF and hy-BZT/PVDF composite film were found to be 1670 kV/cm and 1754 kV/cm respectively. Measurement of PE loop upto breakdown strength value of composite is not possible for us due to the limitation of applied voltage and thickness of sample. The calculated value of energy storage density for hy-BZT/PVDF was found to be 0.41 J/cm^3 at electric field of 790 kV/cm.

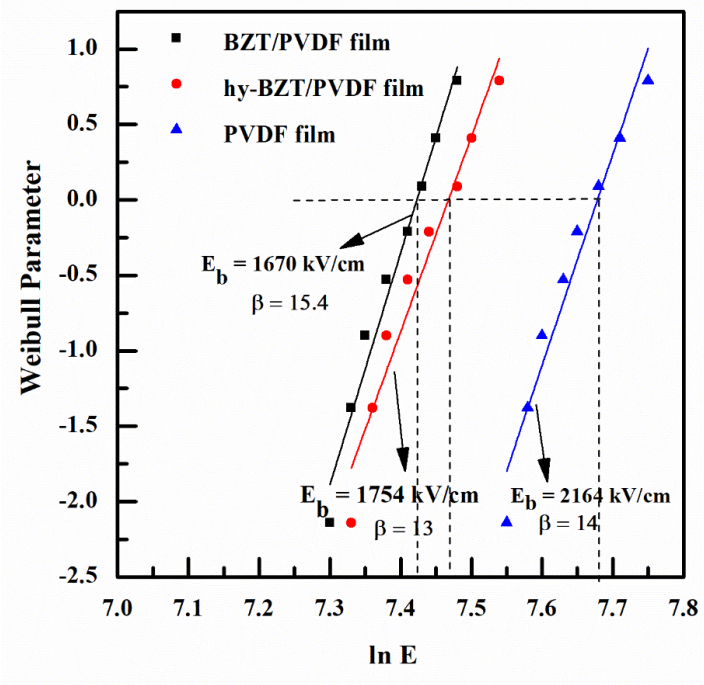

Fig. 5.13 Weibull analysis for pure PVDF film, BZT/PVDF composite and hy-BZT/PVDF composite film

Table 5.2 Comparison of the dielectric permittivity and energy storage density of different reported PVDF based Composites with hy-BZT/PVDF composite film.

Sample Name	**Dielectric permittivity**	**Energy storage density (J/cm^3)**	**Reference**
PVDF/hy-$GdFeO_3$	15.15	0.294	[142]
PVDF/hy-$BiFeO_3$	15	0.145	[123]
PVDF/Ag@$BaTiO_3$	20	0.83	[203]
BZT/PVDF	**12**	**0.37**	**Present work**
hy-BZT/PVDF	**25.5**	**0.41**	**Present work**

5.4 Conclusion

Pure PVDF, BZT/PVDF and hy-BZT/PVDF composite films have been synthesized using solution casting method. FTIR spectra of hy-BZT powder confirms the successful

functionalization of ceramic particle. FTIR spectra and XRD analysis confirms the formation of dominant polar phases of PVDF and suppression of nonpolar phase and better degree of crystallinity was confirmed from DSC plot which is good sign for energy storage application. The significantly improved dielectric properties ($\varepsilon_r \sim 25.5$) has been obtained in case of hy-BZT/PVDF composite film in comparison to pure PVDF film ($\varepsilon_r \sim 8$). Ferroelectric properties of composites have been also improved in comparison to PVDF. We have calculated energy storage density using Weibull analysis for hy-BZT/PVDF composite and was found to be 0.41 J/cm^3 at electric field of 790 kV/cm.